Chemosphere 241 (2020) 124985

Contents lists available at ScienceDirect

Chemosphere

journal homepage: www.elsevier.com/locate/chemosphere

Chemical speciation, distribution and leaching behavior of chlorides from municipal solid waste incineration bottom ash

Qadeer Alam [a, *], Alberto Lazaro [a], Katrin Schollbach [a, b], H.J.H. Brouwers [a]

[a] Department of the Built Environment, Eindhoven University of Technology, P. O. Box 513, 5600, MB, Eindhoven, the Netherlands
[b] Tata Steel, R&D, Microstructure & Surface Characterization (MSC), P. O. Box 10.000, 1970, CA, Ijmuiden, the Netherlands

HIGHLIGHTS

- The chemical speciation of chloride in MSWI bottom ash is reported.
- Halite (NaCl) is major soluble Cl^- in coarser bottom ash particles (0.125 −4 mm).
- Cl^- is immobilized by hydrous Al-oxides, ettringite & melilitic incineration slag.
- Cl^- leaching profiles (upto 80 h) from BA are obtained with chloride ion specific electrode.
- Leaching of Cl^- from BA is both diffusion- and reaction-controlled phenomenon.

GRAPHICAL ABSTRACT

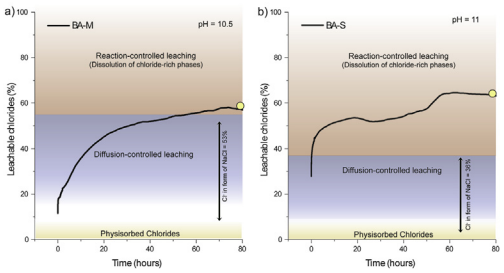

ARTICLE INFO

Article history:
Received 29 March 2019
Received in revised form
24 September 2019
Accepted 26 September 2019
Available online 27 September 2019

Handling Editor: X. Cao

Keywords:
Chloride speciation
Leaching
Bottom ash
MSWI
Washing treatments

ABSTRACT

Municipal solid waste incineration (MSWI) bottom ash is an environmentally harmful solid waste that cannot be recycled without pre-treatment. The chloride content in bottom ash (BA) is a major obstacle that restricts its application as secondary building materials. Here, the chemical speciation of the chlorides in BA is systematically studied with multiple analytical techniques, i.e., quantitative XRD, microanalysis and XPS. In addition to halite (NaCl), several chloride-rich minerals are present in BA. These phases are hydrous metal oxides, ettringite, decomposed hydration products (C_4A_3) and incineration slag with a chloride content of 3.2%, 1.4%, 2.1% and 1.3%, respectively. For the first time, the real-time leaching profiles of chloride (up to 80 h) from BA were obtained with a chloride-ion specific electrode to explain the leaching mechanism. In the initial stage of leaching, highly soluble alkali salts (NaCl) and physisorbed chlorides (especially those adsorbed on hydrous metal oxides) are released, which is controlled by diffusion. Later, the leaching is controlled by the solubility/reactivity of the chloride-containing phases, such as ettringite and incineration slag. The results show that the release of chloride is not only a diffusion-controlled process, as reported in the literature, but also a reaction-controlled phenomenon, during which the chloride-rich phases decompose and release chlorides that are associated with them via sorption/incorporation.

1. Introduction

Municipal solid waste incineration (MSWI) is increasing rapidly due to anthropogenic activities and urbanization. In the

* Corresponding author.
E-mail address: q.alam@tue.nl (Q. Alam).

https://doi.org/10.1016/j.chemosphere.2019.124985

Netherlands, more than 5.6 million tonnes of the household waste was incinerated in waste-to-energy plants in 2016, which represent an increase of 76% as compared to the waste incinerated in 2010 (Eurostat, 2019). The recycling of bottom ash (BA), which is a major by-product of incineration, is encouraged by the zero waste program of the EU Commision (2014). With exception of a few high-end applications, e.g., synthesis of silica (Alam et al., 2019a), zeolites (Chiang et al., 2014), BA is mainly used as a secondary raw material in the building materials industry (Caprai et al., 2018; Norgaard et al., 2019). However, the content of chlorides in BA is the major challenge for their reuse in building materials. The chloride content is strictly regulated for secondary building materials because they are considered harmful for both the environment and concrete structures (Soil Quality Decree, 2013), because of their ability to increase the corrosion of the steel reinforcements (Lynn et al., 2016). Therefore, before the application of BA as a building material, the chloride content needs to be lowered via pre-treatments.

In MSWI bottom ash, the content of chlorides varies from 0.2 to 5 wt% (Yang et al., 2014). However, in order to use these ashes as aggregate in non-shaped building materials, a leachable chloride content of less than 0.06 wt% is required (Soil Quality Decree, 2013). To reduce Cl^- content washing and thermal treatments are employed (Chandler et al., 1997). Thermal treatments are less frequently applied because they require high temperatures of above 500 °C (Chen et al., 2012; Li et al., 2014). On the other hand, treatments based on the wet-extraction of Cl^- are more effective and economically feasible (Zhu et al., 2010). Therefore, washing treatments to reduce the content of chlorides from incineration residues have been extensively investigated (Alam et al., 2017; Boghetich et al., 2005; Yang et al., 2012). The dissolution of chlorides during the washing treatments depends upon their chemical nature and wet-extraction of Cl^- is only effective for removing fully and sparingly soluble chloride species. Therefore multiple washing steps are often required to reduce the content of chlorides below the permissible regulatory limits (Soil Quality Decree, 2013). Moreover, the chemical speciation of chlorides is rarely investigated and often only X-ray diffraction data is used for identification of the chloride salts. The chemical form of the Cl^- in the ash is indicated to be halite (NaCl) and sylvite (KCl) via qualitative powder X-ray diffraction (Inkaew et al., 2016; Kowalski et al., 2017; Yu et al., 2013). However, BA has a complex mineral composition and the diffraction patterns of the minerals often overlap, thus making the qualitative/quantitative analysis of X-ray diffraction data challenging. Specifically, diffraction patterns of the alkali salts partially overlap with ettringite or melilite and both of these minerals are frequently found in MSWI bottom ash (Alam et al., 2019c; Yang et al., 2014). The leaching behavior of chlorides from BA indicates that in addition to the highly soluble alkali salts other sparingly soluble mineral phases containing chlorides such as Friedel salt (Yang et al., 2014; Yao et al., 2015) are also present. During the washing experiments, the release of the chlorides is often reported to increase with the volume of washing water (Alam et al., 2017; Boghetich et al., 2005; del Valle-Zermeño et al., 2014; Yang et al., 2012), which is contrary to the leaching behavior of the alkali salts that are highly soluble (e.g., the solubility of NaCl in water: 340 g/L at 25 °C). The leaching of chlorides from BA is primarily considered to be controlled by a diffusion process due to the high solubility of alkali salts in aqueous media (Sabbas et al., 2003). In doing so, the role of other BA mineral phases in immobilizing the chloride ions (via sorption/incorporation) is often overlooked. Therefore, understanding the chemical nature of chlorides and their leaching mechanism is of crucial importance in order to design efficient washing treatments requiring less amount of water and shorter treatment times.

In this study, the chemical nature, distribution and leaching behavior of chlorides are investigated and the role of mineral and amorphous phases from MSWI bottom ash in immobilizing chlorides (co-precipitation/sorption) is illustrated. The mineral composition of BA is determined with quantitative XRD via Rietveld method. Microanalysis (SEM/EDX) is used to quantify the content of chlorides associated with the various phases. The chemical speciation is also studied with X-ray photoelectron spectroscopy (XPS). The speciation data of chloride is complemented with the real-time leaching profiles measured with a chloride-ion specific electrode. From these experiments, the leaching behavior of chloride from MSWI bottom ash is reported.

2. Materials and methods

2.1. Materials

Bottom ash with the particle size below 4 mm was provided by Heros Sluiskil, the Netherlands. This particle size range of BA was selected because it contains a high content of chlorides as compare to bigger particles (Alam et al., 2016; Tang et al., 2015; Yang et al., 2014) and therefore considered most problematic. The as-received sample of BA was further separated based on particle size into three fractions, namely: S (≤0.125 mm), M (0.125–1 mm) and L (1–4 mm) by using conventional sieving according to DIN EN 933-1.

2.2. Chemical analyses

The overall chemical composition of the BA fractions was determined with the X-ray fluorescence spectrometer (XRF; PANalytical Epsilon 3) by measuring fused beads. The sample of BA was ignited at 1000 °C to for the loss on ignition (LOI) and subsequently, the part of the residues was mixed with flux (Li_2BO_7 and $LiBO_4$) and non-wetting agent (LiBr). The mixture was melted at 1100 °C in a fluxer over (classisse leNeo) and then cast to obtained glassy fused bead for the XRF analysis.

The quantification of mineral phases was performed with quantitative X-ray diffraction (XRD) via Rietveld refinement. The sample for analysis was prepared by adding 10 wt% of Si as an internal standard. The XRD patterns were measured with Bruker D2 diffractometer equipped with Co as a radiation source, LynxEye detector, divergence and soller slits of 0.2° and 2.5°, respectively. The quantification of mineral phases was performed with the TOPAS 4.2 software (Coelho, 2018).

Polished cross-sections of bottom ash fractions were prepared for the scanning electron microscope (SEM; JEOL JSM-7001F) imaging and energy dispersive X-ray spectroscopy (EDX; Thermo Fisher Scientific). The samples for these measurements are prepared in the absence of water to avoid dissolution of chlorides. The processing of the spectral imaging datasets was performed with the PhAse Recognition and Characterization (PARC) software (Alam et al., 2019c; van Hoek et al., 2016, 2011). Furthermore, the chemical speciation of chlorides was determined with X-ray photon spectroscopy (XPS; Thermo Scientific K-Alpha). The S fraction was used for the qualitative analysis of chlorides because it contained the highest content of chlorides. Furthermore, the chloride content in all the fractions of BA was quantified with instrumental neutron activation analysis (INAA) (Alam et al., 2017).

2.3. Chloride ion specific electrode

The leaching of chlorides from the bottom ash fractions was measured with the help of a solid-state chloride ion specific

electrode (ISE) attached to a Metrohm 785 DMP Titrino. The measurement setup was equipped with the reference electrode and a temperature sensor (Pt1000, Metrohm). A standard solutions of sodium chloride with the concentration ranging from 0.01 to 0.21 M were used for the calibration of the electrode. Additionally, 2 vol% of 5 M $NaNO_3$ was added to the standard solutions as a total ionic strength adjustment buffer. In Fig. A1 (Appendix A) the calibration curves of ISE are given, which show the measured points as a function of the logarithm of chloride ions activity.

For the measurement, a sample of BA was added to deionized water with a liquid-to-solid (L/S) ratio of 3. Afterwards the mixture was stirred for 30 s and subsequently electrodes and temperature sensor were dipped in the mixture. For all experiments, the same protocol was followed. The chloride ions activity was measured for at least 80 h and the data points were collected with two different intervals. For the first 2 h, one set of data points was measured with an interval of 30 s and afterwards, another set of data points was collected every 20 min. Once the measurements were finished, an aliquot of liquid was collected from the container and the chloride content was measured with ion-chromatography. Before every analysis, the electrode was cleaned and calibrated to take into account the effect of ageing and hysteresis. Subsequently, the calibration was used for the determination of the chloride concentration.

2.4. Ion chromatography

An ion chromatograph (Thermo scientific Dionex 1100) equipped with ion exchange column AS9-HS (2 × 250 mm) was used. Na_2CO_3 solution (9 mM) was used as an eluent and chlorides ions were detected with the electrolytically regenerated suppressor (Thermo scientific Diones AERS 500, 2 mm). The contents of the chlorides measured with IC were compared with the chloride content obtained from ISE. The comparison was performed to ensure the accuracy of the results and correct for the possible drift in the signal of chloride ion-specific electrode.

3. Results and discussion

3.1. Characterization of bottom ash

The chemical composition of the BA fractions is provided in Table 1. The major oxides are CaO, SiO_2, Al_2O_3 and Fe_2O_3 representing between 60 and 80 wt% of the chemical composition of all three fractions. The minor elements in BA are Cu, Zn, Cr, Sb, Mo, Co and Ni, etc., and make up about 1.5–2.0 wt% along with 1.5–5.0 wt% of chlorides and sulfates, depending on the size fraction of BA. The content of chloride increases with the decrease in the particle size of bottom ash; a similiar trend for is already reported in the literature (Caviglia et al., 2019; Yang et al., 2014). The highest chloride content (1.2 wt%) was observed in the BA-S fraction.

In Table 2, the mineral phases present in the BA fractions and their quantification is provided. These minerals are categorized as residual, incineration or weathering phases based on their origin/source. The residual phases (e.g., quartz, apatite) are present already in the original waste feed and remain unaffected by the incineration. The incineration phases are formed under the incineration conditions such as melilite, pyroxene and iron oxides. Lastly, the weathering phases are the product of water-quenching and carbonation processes and include calcite, ettringite, and gypsum. The BA-M and BA-L fractions are similar to each other in their mineral composition. However, the smallest fraction, BA-S, shows a different composition as compared to the rest of the fractions. The BA-S fraction is enriched with the weathering phases, i.e., calcite, ettringite and gypsum (Alam et al., 2019c).

Table 2
Mineralogical composition (wt.%) of the size-separated bottom ash fractions, BA-S (≤125 μm), BA-M (0.125–1 mm) and BA-L (1–4 mm) measured via quantitative XRD.

Minerals (wt.%)	BA-S	BA-M	BA-L
Apatite	5.2	6.8	6.2
Calcite	25.6	14.8	10.8
Chabazite	2.1	–	–
Ettringite	4.1	–	–
Gypsum	5.4	–	–
Halite	0.7	0.8	0.7
Hematite	2.2	3.8	4.0
Melilite	3.0	4.4	5.3
Plagioclase	3.9	5.3	6.3
Pyroxene	1.3	3.5	5.4
Quartz	6.6	15.7	9.3
Rutile	1.0	1.2	1.4
Spinel	3.8	8.1	10.5
Wuestite	–	1.4	1.7
Amorphous	34.9	34.2	38.4
Sum	100	100	100

The only chloride-containing mineral identified in the BA fractions is halite (NaCl) and its content ranged between 0.7 and 0.8 wt %. The halite content in the BA-L, BA-M and BA-S fractions accounts for 36%, 53% and 61% of the total chloride, respectively. The XRD data of the bottom ash fractions only provides information about the well crystalline chloride salts, i.e., halite. The rest of the chlorides are either in amorphous form or associated with other mineral phases of BA. For this reason microanalysis was performed, to investigate the distribution and interactions (via sorption/incorporation) of chlorides with the BA phases.

3.2. Chemical nature and distribution of chlorides

The distribution of the chlorides in the matrix of BA is an important factor for determining their mobility during leaching. An SEM image of the polished section of the original BA with a particle size below 4 mm is provided in Fig. 1a. In this sample, the presence of metallic particles, a residual phase (quartz) and incineration slag is observed. The particles of BA are covered with the slag that is produced during the incineration. A chlorine map (measured via EDX) showing the distribution of the anion in the original as received BA fraction (≤4 mm) is given in Fig. 1b. The majority of the chlorides are coating the particle surface just like the incineration slag. The inner core of the particles does not contain chlorides (except the particle present on the lower left of Fig. 1b.) that ensure

Table 1
Chemical composition (in wt.%) of the three bottom ash fractions separated based on particle size, BA-S (≤125 μm), BA-M (0.125–1 mm) and BA-L (1–4 mm) measured with XRF. R.O.: Remaining oxides, LOI: Loss on ignition at 1000 °C.

(wt.%)	CaO	SiO_2	Al_2O_3	Fe_2O_3	SO_3	MgO	P_2O_5	TiO_2	ZnO	K_2O	Sb_2O_3	CuO	R.O.	LOI	Cl[a]
BA-S	25.0	19.5	12.6	6.3	3.7	1.7	1.6	1.4	0.8	0.5	0.3	0.2	0.5	25.8	1.19 ± 0.13
BA-M	17.4	36.9	10.9	12.6	1.0	1.7	1.4	1.3	0.6	0.9	0.1	0.4	0.5	14.3	0.85 ± 0.10
BA-L	18.7	37.2	11.7	14.4	0.9	2.6	1.6	1.3	0.6	1.2	0.1	0.3	0.5	8.7	0.65 ± 0.05

[a] The content of chlorides is measured with the instrumental neutron activation analysis.

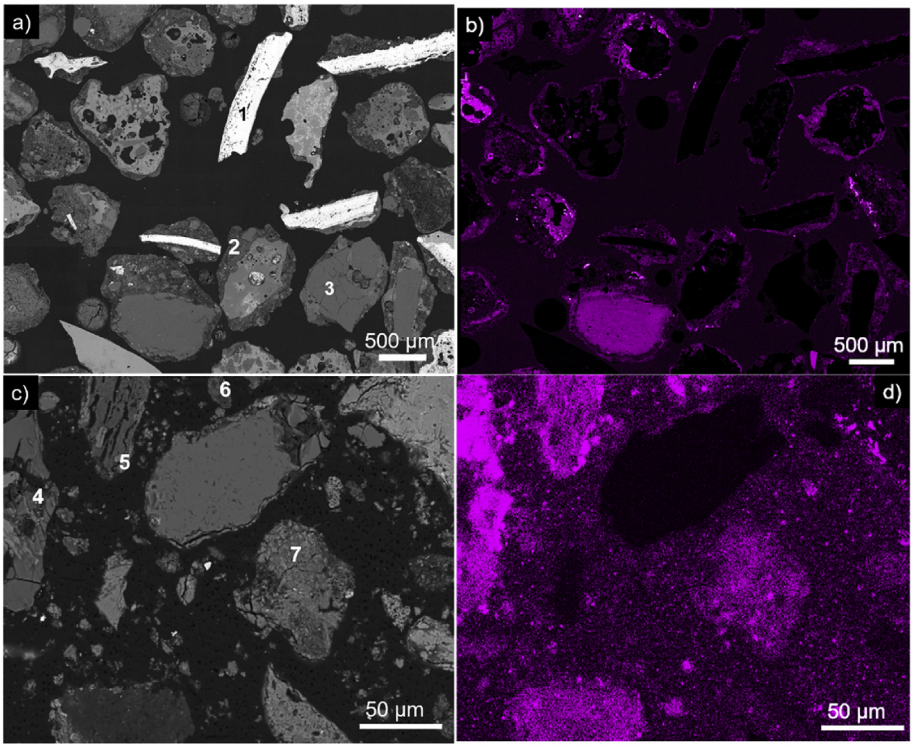

Fig. 1. a) SEM image of the polished sample of the original bottom ash fraction (≤4 mm), b) EDX map of chlorides for the original BA fraction, c) SEM image for the BA-S fraction (≤0.125 mm) and d) chloride mapping of BA-S. The numbered areas on the SEM images are 1 – metallic particles, 2 – incineration slag, 3 – precursor phases, 4 – hydrous Al-oxides, 5 – MCA-Cl, 6 – C_3A_4 and 7 – ettringite.

the maximum contact with the water during leaching.

An SEM image of the polished sample of BA-S (125 µm) and its respective chlorine map is provided in Fig. 1c and d. The BA-S fraction is chosen for the chlorine mapping because it contains the highest content of chlorides as compared to rest of the fractions. Moreover, only one-third of the chlorides in this fraction are present as halite, which provides an opportunity to study the other chloride-rich mineral phases of BA. Unlike the original fraction of BA (≤4 mm) in which chlorides are coating the particle surface, in BA-S the chlorides are present throughout the particles and there is no distinction between an outer layer and a core. Several chloride-rich areas are observed in Fig. 1c and they were numbered 4–7. The chemical composition of these areas was analyzed to illustrate the association between chlorides and mineral phases of BA.

The chemical composition of the chloride-rich phases from the BA-S fraction is obtained with PARC (PhAse Recognition and Characterization) analysis (Alam et al., 2019c; van Hoek et al., 2016). The summed EDX spectra of these phases are provided in Fig. 2 and their respective chemical composition is given in Table 3. The majority of the chloride-rich phases are produced during either incineration or weathering processes. These phases were named as a mineral if their composition matched with the mineral identified via XRD. If the composition does not correspond with any mineral observed with XRD, then they were named according to the cement chemistry notation based on the ratio of their major elements.

The chloride-rich mineral phases from BA include hydrous Al-oxides, C_3A_4 (calcium aluminate), MCA-Cl (unspecified phase rich in Mg, Ca, Al and Cl), ettringite and melilite (incineration slag). The presence of hydrous metallic oxides of aluminium and iron and their role in the leaching of heavy metals is frequently reported in the literature (Jeannet A. Meima and Comans, 1998). However, their role with respect to the leaching of chlorides is often overlooked. The hydrous Al-oxide (74 wt% Al_2O_3) from the BA-S fraction contains 3.2 wt% Cl. These hydrous oxides can immobilize chloride ions from their surrounding via sorption. Other phases, such as ettringite and C_4A_3 contain 2.1 and 1.4 wt% of chlorides, respectively. The C_4A_3 phase is the decomposition product of monosulfate, which is formed because of the carbonation of the ettringite originating from the hydration of C_3A (tricalcium aluminate) (Norgaard et al., 2019). C_3A is formed during incineration of MSW and its hydration takes place when the ash is water-quenched (Inkaew et al., 2016), as explained in Section 4.3.2. Ettringite is a well-known weathering phase that is formed in BA with the general chemical formula of X_6 $[Y_2(OH)_{12}\cdot 24\,H_2O]$ $[T_3\cdot nH_2O]$. The T-position is typically occupied by sulfates, but can also accommodate chloride ions (Gougar et al., 1996). Furthermore, the chemical composition of ettringite given in Table 3 shows 5.3 wt% of SiO_2. It could be either incorporated in the crystal structure at the Y-position or just physically intermixed. The incineration slag produced during the incineration of municipal solid waste contains 1.3 wt% of chlorides. The mineral phase with the highest content of chlorides (11.5 wt%) is MCA-Cl. The major elements in this phase are Mg, Ca, and Al and its stoichiometry does not correspond with any mineral identified with XRD, indicating its amorphous nature.

The most abundant form of chloride in all three fractions of BA is halite (NaCl), as determined via quantitative XRD. The XPS spectrum of Cl 2p from the BA-S fraction of bottom ash is provided in Fig. 3. The spectrum shows the binding energy for Cl $2p_{3/2}$ at 197.9 eV and a shoulder for Cl $2p_{1/2}$ at 199.5 eV from the spin-orbit splitting of the 2p level. The binding energy of the Cl $2p_{3/2}$ bound in the sodium chloride state is reported to be at 198 eV (Wagner et al., 1995). The presence of a similar peak for the binding energy of Cl $2p_{3/2}$ in BA-S confirms the existence of sodium chloride in MSWI bottom ash as indicated by the X-ray diffraction data.

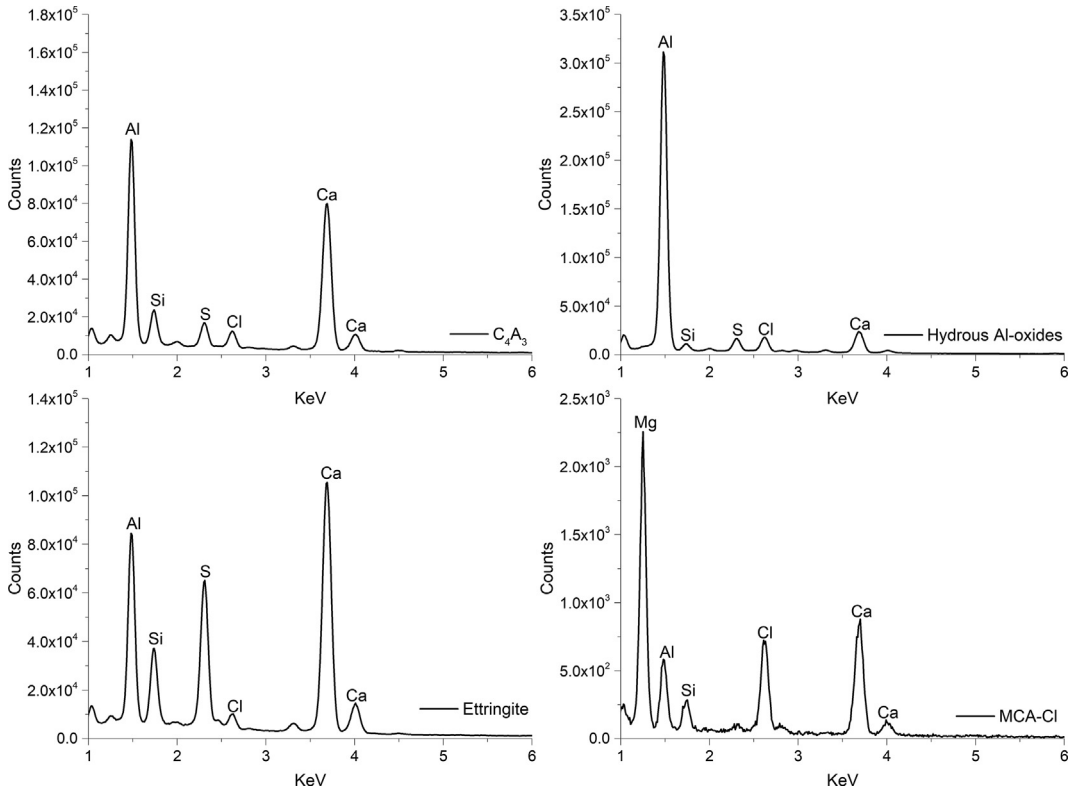

Fig. 2. Summed EDX spectra for phases (C_4A_3, hydrous Al-oxides, ettringite and MCA-Cl) from the BA-S fraction of bottom ash (≤125 μm) obtained via PARC (PhAse Recognition and Characterization) software.

Table 3
The chemical composition of the chloride-rich phases obtained via summed EDX spectra processed via the PARC software. C_4A_3, MCA-Cl: unspecified chloride rich phase. The chloride content is relative to the composition of the phase.

Phase	Hydrous Al-oxides	C_4A_3	MCA-Cl	Ettringite	Melilite
Al_2O_3	74.2	30.3	10.9	17.5	18.1
CaO	8.0	49.0	31.1	41.4	33.2
Cl	3.2	2.1	11.5	1.4	1.3
FeO	0.7	1.3	1.4	0.9	5.9
K_2O	0.7	0.6	0.4	0.5	1.0
MgO	0.1	0.6	31.2	0.2	2.4
Na_2O	1.9	1.4	0.7	0.9	2.4
P_2O_5	1.1	0.7	0.9	0.1	1.5
SiO_2	2.8	5.3	5.6	5.1	28.4
SO_3	5.5	6.3	1.6	30.9	3.1
Others	1.7	2.3	4.7	1.2	2.8

3.3. Dissolution behavior of chlorides

The dissolution behavior of chlorides from the size-separated fractions, BA-M (0.125–1 mm) and BA-S (≤0.125 mm) was monitored and real-time leaching profiles of chloride are provided in Fig. 4. These profiles were measured with a liquid-to-solid (L/S) ratio of three at 20 °C. The mineral composition of the BA-M fraction is similar to BA-L. Therefore, only data from the BA-M fraction is discussed. Upon contact with water, approximately 12.5% of chlorides are released in water immediately (see Fig. 4a). The leaching of chlorides from the BA-M fraction increases with time and reaches a plateau at around 60 h. It is important to note that the mixture was left undisturbed to avoid unnecessary interferences with the ISE. The content of chloride bound in the form of halite in the BA-M fraction is 53% and the total content of chloride dissolved

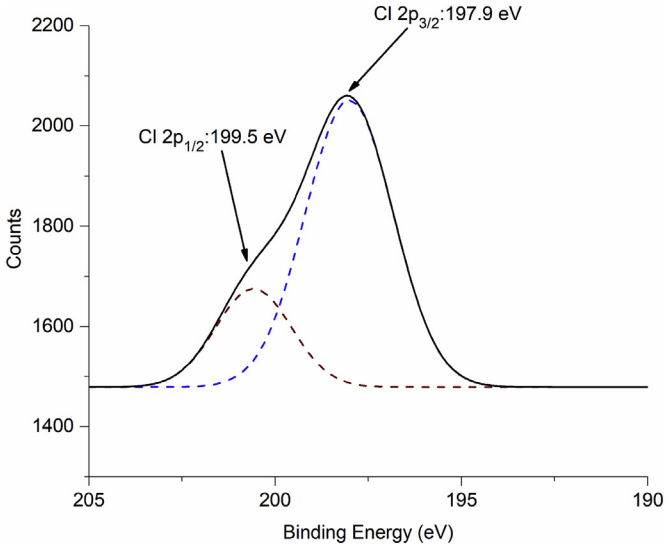

Fig. 3. X-ray photoelectron spectrum is showing the binding energy for Cl 2p from the BA-S (≤125 μm) fraction of bottom ash.

after 80 h is 57%. The real-time dissolution profile of chloride from the BA-M fraction confirms that the major soluble chloride is halite (NaCl) and its release in an aqueous medium is diffusion-controlled. The rest of the chlorides account for 43% and are immobilized in mineral phases of BA via both sorption or crystal structure incorporation and their release depends on the reactivity of those phases. Due to the high water adsorption capacity of BA (Caprai et al., 2019), it will retain a part of the chloride-containing washing

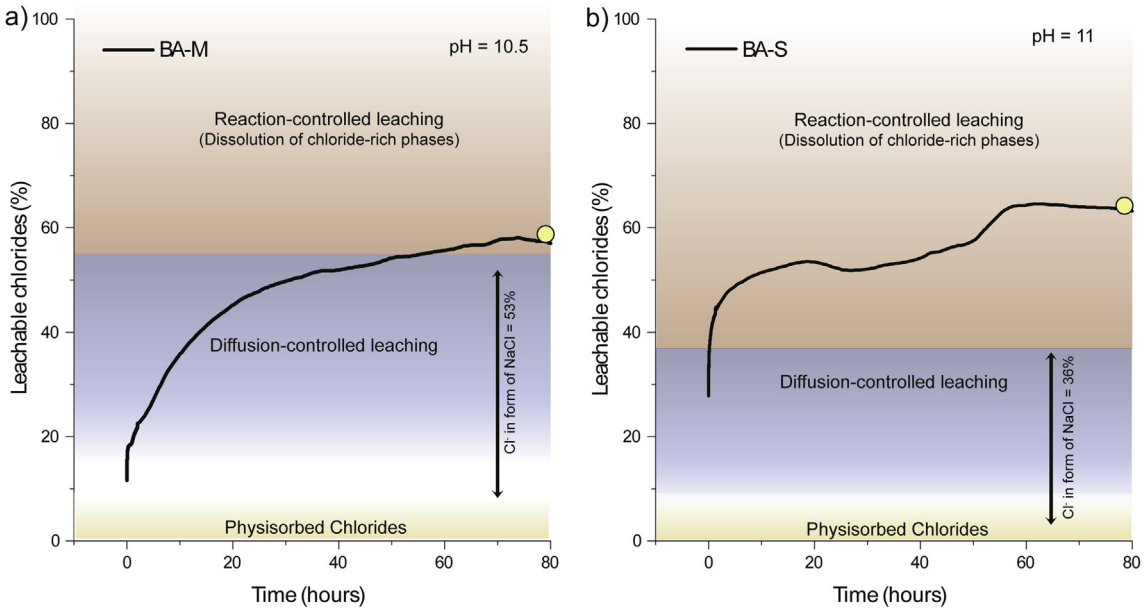

Fig. 4. The real-time dissolution profiles of chlorides from the two fraction of bottom ash, **a)** BA-M (0.125–1 mm) and **b)** BA-S (≤0.125 mm). The yellow dot shows the chloride content determined via IC at the end of the experiment. Each curve contained more than 750 data points obtained via chloride ions specific electrode with a liquid-to-solid ratio of three (L/S = 3) at 20 °C. (For interpretation of the references to colour in this figure legend, the reader is referred to the Web version of this article.)

water during the separation. In the literature, multiple washing steps are frequently reported to obtain higher extraction efficiency of chlorides (Alam et al., 2017; Yang et al., 2012). Initially, the first washing step extracts highly soluble Cl^- (physisorbed/halite) and this step is diffusion controlled. Subsequent washing steps remove residual soluble chlorides as well as chlorides that are associated with mineral phases with low solubilities, such as incineration slag and ettringite. The release of chlorides after the first washing step is mainly reaction controlled. Therefore, multiple-step washing treatments with lower liquid-to-solid ratio are more effective (Alam et al., 2017) in removing Cl^- because the initial step extracts highly soluble, physisorbed chloride species and subsequent washing steps can remove sparingly soluble chlorides that are associated with the mineral phases of BA.

The chloride dissolution profile from the BA-S fraction (≤0.125 mm) is provided in Fig. 4b. The dissolution behavior of chlorides from this fraction is different as compared to the BA-M fraction. More than 28% of the chlorides are dissolved within the first hour. The chloride content in the form of halite in this fraction accounts for 36% and their release fast primarily due to the higher surface area of the ash particles (32 m^2/g, measured with nitrogen physisorption) and the lack of a rim/core structure of particles. In addition to that, the BA-S fraction contain other chlorides-containing phases such as hydrous Al-oxides (see Table 3). These hydrous oxides physisorbed Cl^-, which are released in an aqueous medium. After 20 h, a dip in the concentration of the chlorides was observed. The decomposition of weathering phases such as ettringite, gypsum and hydration products occur in an aqueous environment (Alam et al., 2019b, 2017) and that could lead to the temporary immobilization of chlorides via physisorption. Afterwards, the chloride content in water increases steadily and reaches a plateau at around 60 h. In the case of BA-S, the chloride leaching in early stages is because of the dissolution of halite and release of physisorbed chlorides (from hydrous metal oxides). Once highly soluble and physisorbed chlorides are in the solution, the release of chlorides depends on the dissolution of weathering and incineration phases. Almost two-thirds of chlorides in this fraction are immobilized by mineral phases (e.g., melilite, ettringite) of BA and their release is controlled by the reactivity of these chloride-containing minerals.

4. Conclusions

The chemical nature of the chlorides and their dissolution behavior from size-separated MSWI bottom fraction is systematically investigated with multiple analytical tools and the key finding are as follows:

- Size-separated fraction of bottom ash; namely, BA-S (≤0.125 mm), BA-M (0.125–1 mm) and BA-L (1–4 mm) contained halite (NaCl) which accounted for 62%, 53% and 36% of the total chlorides, respectively.
- In the coarser BA fractions, chlorides are mainly present in a surface layer, which is coating the BA particles, while the core of these particles does not contain any chloride. Only in the case of fines (≤0.125 mm), are the chlorides dispersed throughout the particles.
- The main chloride-containing phases in BA-S besides halite are hydrous Al-oxides, ettringite, decomposed hydration products (C_3A_4) with 3.2%, 1.4%, and 2.1% of chlorides, respectively.
- The dissolution of chlorides from the MSWI bottom ash is both a diffusion and reaction controlled process. Initially, most soluble chloride species (e.g., halite) and physisorbed chlorides (especially on hydrous metal chlorides) are dissolved, which can be classified as diffusion-controlled leaching. Afterwards, the chloride release depends on the solubilities/decomposition reactions of the weathering phases and incineration slag (given in order of decreasing reactivity).

Declaration of competing interest

None.

Acknowledgements

The authors would like to acknowledge the financial support provided by NWO (Nederlandse Organisatie voor Wetenschappelijk Onderzoek), the Netherlands, under the project number 10019729: "Environmental concrete based on the treated MSWI bottom ashes". The authors are thankful for the assistance provided by prof. dr. S. R. van der Laan and Mrs. C. van Hoek for the PARC measurements and ing. C.A.A. van Helvoirt for the XPS measurements. Also, special thanks to Mrs. V. Caprai for designing Fig. 4 of this manuscript.

Appendix A. Supplementary data

Supplementary data to this article can be found online at https://doi.org/10.1016/j.chemosphere.2019.124985.

References

Alam, Q., Schollbach, K., Florea, M.V.A., Brouwers, H.J.H., 2016. Investigating washing treatment to minimize leaching of chlorides and heavy metals from MSWI bottom ash. In: 4th International Conference on Sustainable Solid Waste Management. Limassol, Cyprus.

Alam, Q., Florea, M.V.A., Schollbach, K., Brouwers, H.J.H., 2017. A two-stage treatment for Municipal Solid Waste Incineration (MSWI) bottom ash to remove agglomerated fine particles and leachable contaminants. Waste Manag. 67, 181–192. https://doi.org/10.1016/J.WASMAN.2017.05.029.

Alam, Q., Hendrix, Y., Thijs, L., Lazaro, A., Schollbach, K., Brouwers, H.J.H., 2019a. Novel low temperature synthesis of sodium silicate and ordered mesoporous silica from incineration bottom ash. J. Clean. Prod. 211, 874–883. https://doi.org/10.1016/J.JCLEPRO.2018.11.173.

Alam, Q., Schollbach, K., Rijnders, M., van Hoek, C., van der Laan, S., Brouwers, H.J.H., 2019b. The immobilization of potentially toxic elements due to incineration and weathering of bottom ash fines. J. Hazard Mater. 379, 120798. https://doi.org/10.1016/J.JHAZMAT.2019.120798.

Alam, Q., Schollbach, K., van Hoek, C., van der Laan, S., de Wolf, T., Brouwers, H.J.H., 2019c. In-depth mineralogical quantification of MSWI bottom ash phases and their association with potentially toxic elements. Waste Manag. 87, 1–12. https://doi.org/10.1016/J.WASMAN.2019.01.031.

Boghetich, G., Liberti, L., Notarnicola, M., Palma, M., Petruzzelli, D., 2005. Chloride extraction for quality improvement of municipal solid waste incinerator ash for the concrete industry. Waste Manag. Res. 23, 57–61. https://doi.org/10.1177/0734242X05051017.

Caprai, V., Schollbach, K., Brouwers, H.J.H., 2018. Influence of hydrothermal treatment on the mechanical and environmental performances of mortars including MSWI bottom ash. Waste Manag. 78, 639–648. https://doi.org/10.1016/J.WASMAN.2018.06.030.

Caprai, V., Lazaro, A., Brouwers, H.J.H., 2019. Waterglass impregnation of municipal solid waste incineration bottom ash applied as sand replacement in mortars. Waste Manag. 86, 87–96. https://doi.org/10.1016/J.WASMAN.2019.01.025.

Caviglia, C., Confalonieri, G., Corazzari, I., Destefanis, E., Mandrone, G., Pastero, L., Boero, R., Pavese, A., 2019. Effects of particle size on properties and thermal inertization of bottom ashes (MSW of Turin's incinerator). Waste Manag. 84, 340–354. https://doi.org/10.1016/J.WASMAN.2018.11.050.

Chandler, R.T., Eighmy, T.T., Hertlen, J., Hjelmar, O., Kosson, D.S., Sawel, S.E., van der Sloot, H.A., Vehlow, J., 1997. Municipal Solid Waste Incinerator Residues - IAWG (International Ash Working Group). Elsevier.

Chen, W.-S., Chang, F.-C., Shen, Y.-H., Tsai, M.-S., Ko, C.-H., 2012. Removal of chloride from MSWI fly ash. J. Hazard Mater. 237–238, 116–120. https://doi.org/10.1016/j.jhazmat.2012.08.010.

Chiang, Y.W., Santos, R.M., Vanduyfhuys, K., Meesschaert, B., Martens, J.A., 2014. Atom-efficient route for converting incineration ashes into heavy metal sorbents. ChemSusChem 7, 276–283. https://doi.org/10.1002/cssc.201300704.

Coelho, A.A., 2018. *TOPAS* and *TOPAS-Academic*: an optimization program integrating computer algebra and crystallographic objects written in C++. J. Appl. Crystallogr. 51, 210–218. https://doi.org/10.1107/S1600576718000183.

del Valle-Zermeño, R., Chimenos, J.M., Giró-Paloma, J., Formosa, J., 2014. Use of weathered and fresh bottom ash mix layers as a subbase in road constructions: environmental behavior enhancement by means of a retaining barrier. Chemosphere 117, 402–409. https://doi.org/10.1016/J.CHEMOSPHERE.2014.07.095.

EU Commision, 2014. Towards a Circular Economy: A Zero Waste Programme for Europe.

Gougar, M.L.D., Scheetz, B.E., Roy, D.M., 1996. Ettringite and C-S-H Portland cement phases for waste ion immobilization: a review. Waste Manag. 16, 295–303. https://doi.org/10.1016/S0956-053X(96)00072-4.

Inkaew, K., Saffarzadeh, A., Shimaoka, T., 2016. Modeling the formation of the quench product in municipal solid waste incineration (MSWI) bottom ash. Waste Manag. 52, 159–168. https://doi.org/10.1016/j.wasman.2016.03.019.

Kowalski, P.R., Kasina, M., Michalik, M., 2017. Metallic elements occurrences in the municipal waste incineration bottom ash. Energy Procedia 125, 56–62. https://doi.org/10.1016/J.EGYPRO.2017.08.060.

Li, H., Wu, W., Bubakir, M.M., Chen, H., Zhong, X., Liu, Z., Ding, Y., Yang, W., 2014. Polypropylene fibers fabricated via a needleless melt-electrospinning device for marine oil-spill cleanup. J. Appl. Polym. Sci. 131 n/a-n/a. https://doi.org/10.1002/app.40080.

Lynn, C.J., Dhir OBE, R.K., Ghataora, G.S., 2016. Municipal incinerated bottom ash characteristics and potential for use as aggregate in concrete. Constr. Build. Mater. 127, 504–517. https://doi.org/10.1016/j.conbuildmat.2016.09.132.

Meima, Jeannet A., Comans, R.N.J., 1998. Application of surface complexation/precipitation modeling to contaminant leaching from weathered municipal solid waste incinerator bottom ash. Environ. Sci. Technol. 32, 688–693. https://doi.org/10.1021/ES9701624.

Norgaard, K.P., Hyks, J., Mulvad, J.K., Frederiksen, J.O., Hjelmar, O., 2019. Optimizing large-scale ageing of municipal solid waste incinerator bottom ash prior to the advanced metal recovery: phase I: monitoring of temperature, moisture content, and CO2 level. Waste Manag. 85, 95–105. https://doi.org/10.1016/J.WASMAN.2018.12.019.

Sabbas, T., Polettini, A., Pomi, R., Astrup, T., Hjelmar, O., Mostbauer, P., Cappai, G., Magel, G., Salhofer, S., Speiser, C., Heuss-Assbichler, S., Klein, R., Lechner, P., 2003. Management of municipal solid waste incineration residues. Waste Manag. 23, 61–88. https://doi.org/10.1016/S0956-053X(02)00161-7.

Soil Quality Decree, 2013. Regeling Bodemkwaliteit, VROM, Den Haag: Ruimte en Milieu. Ministerie van Volkshuisvesting, Ruimtelijke Ordeling en Milieubeheer).

Tang, P., Florea, M.V.A., Spiesz, P., Brouwers, H.J.H., 2015. Characteristics and application potential of municipal solid waste incineration (MSWI) bottom ashes from two waste-to-energy plants. Constr. Build. Mater. 83, 77–94. https://doi.org/10.1016/j.conbuildmat.2015.02.033.

van Hoek, C.J.G., de Roo, M., van der Veer, G., van der Laan, S.R., 2011. A SEM-EDS study of cultural heritage objects with interpretation of constituents and their distribution using PARC data analysis. Microsc. Microanal. 17, 656–660. https://doi.org/10.1017/S1431927610094390.

van Hoek, C.J.G., Small, J., van der Laan, S.R., 2016. Large area phase mapping using PhAse Recognition and Characterization (PARC) software. Micros. Today 24. https://doi.org/10.1017/S1551929516000572.

Wagner, C.D., Rigges, W.M., Davis, L.E., Moulder, J.F., 1995. Handbook of X-Ray Photoelectron Spectroscopy : a Reference Book of Standard Spectra for Identification and Interpretation of XPS Data. Perkin-Elmer Corporation, Minnesota.

Yang, R., Liao, W.-P., Wu, P.-H., 2012. Basic characteristics of leachate produced by various washing processes for MSWI ashes in Taiwan. J. Environ. Manag. 104, 67–76. https://doi.org/10.1016/j.jenvman.2012.03.008.

Yang, S., Saffarzadeh, A., Shimaoka, T., Kawano, T., 2014. Existence of Cl in municipal solid waste incineration bottom ash and dechlorination effect of thermal treatment. J. Hazard Mater. 267, 214–220. https://doi.org/10.1016/j.jhazmat.2013.12.045.

Yao, J., Kong, Q., Zhu, H., Long, Y., Shen, D., 2015. Retention and leaching of nitrite by municipal solid waste incinerator bottom ash under the landfill circumstance. Chemosphere 119, 267–272. https://doi.org/10.1016/J.CHEMOSPHERE.2014.06.057.

Yu, J., Sun, L., Xiang, J., Jin, L., Hu, S., Su, S., Qiu, J., 2013. Physical and chemical characterization of ashes from a municipal solid waste incinerator in China. Waste Manag. Res. 31, 663–673. https://doi.org/10.1177/0734242X13485793.

Zhu, F., Takaoka, M., Oshita, K., Kitajima, Y., Inada, Y., Morisawa, S., Tsuno, H., 2010. Chlorides behavior in raw fly ash washing experiments. J. Hazard Mater. 178, 547–552. https://doi.org/10.1016/j.jhazmat.2010.01.119.

Eurostat, 2009. Treatment of waste by waste category, hazardousness and waste management operations. Eurostat. (Accessed 14 May 2019).